This is a postprint of: Electrochimica Acta 129 (2014) 160-170

ELECTROCHEMICAL STUDY ON THE CORROSION BEHAVIOUR OF A NEW LOW-NICKEL STAINLESS STEEL IN CARBONATED ALKALINE SOLUTION IN THE PRESENCE OF CHLORIDES

S. Fajardo[*, 1], D. M. Bastidas, M. Criado and J. M. Bastidas

National Centre for Metallurgical Research (CENIM), CSIC

Avda. Gregorio del Amo 8, 28040 Madrid, Spain

Abstract

An electrochemical study was performed on a low-nickel stainless steel (SS) in order to evaluate its corrosion behaviour. The conventional AISI 304 SS was also studied for comparative proposes. A carbonated alkaline solution was used as electrolyte. The effect of carbonation and the combined effect of carbonation and the presence of chloride ions were studied. The low-nickel SS exhibited similar corrosion behavior to the conventional AISI 304 SS with corrosion potential and charge transfer resistance of the same order while the pitting potential were slightly lower. Corrosion current density supported these results with very similar values between the two studied SSs.

Key Words: Low-nickel stainless steel; carbonation; polarization; EIS; passivity.

[*]Corresponding Author, Tel.: +34 91 553 8900; Fax: +34 91 534 7425; E-mail Address: s.fajardo@cenim.csic.es (S. Fajardo).

[1]ISE member.

1 INTRODUCTION

Reinforced concrete structures (RCS) normally present a great corrosion resistance. The high alkaline media, such as that contained in the pores of the concrete (pH about 12–13) promotes the formation of a protective oxide layer on the surface of the steel that prevents it from corrosion [1, 2]. Previous studies have revealed that these passive oxide films, formed of iron and chromium oxides, are of the order of only a few nanometres (nm) thick or even less depending on the time of exposure of the sample to the passivating media [3]. However, the presence of chlorides (Cl^-) can lead to damaging effects on passivity and the appearance of pitting corrosion when chloride ions reach the metal/concrete interface [4]. In addition to this phenomenon, carbonation processes over the solution contained into the pores of the concrete causes severe corrosion problems due to a drop in pH (under the value of 9) that turns the passive state to an active corrosion process [1]. These two factors lead to the corrosion and deterioration of the RCS with the result of a less stable and secure structure and the subsequent costs in maintenance and reparation works.

Among the corrosion protection methods, cathodic protection, corrosion inhibitors and galvanized steel, stainless steel (SS) reinforcements are a reliable way to guarantee the durability of RCS in extremely aggressive environments where carbon steel presents protection limitations [5-7]. Although SS reinforcements may be the most economical solution in the long term [8, 9], the initial cost involved has so far limited their use.

The interest in SS reinforcements is a result of its resistance to a great variety of environments and its property of self-regeneration after partial destruction of its passive film. As a result, structural service-life spans of SS reinforced structures are increased with respect to traditional carbon steel ones [10]. Stainless steel reinforced concrete was

first used in the construction of a pier built in the Gulf of Mexico (Port of Progresso, Yucatán, Mexico), between 1937 and 1941 [11]. The latest inspection of the structure revealed that it is virtually free of corrosion. USA, Canada, Australia and some European countries are currently using SS as reinforcements in RCS.

The SSs most frequently used as reinforcement are the austenitic types AISI 304 and AISI 316. Previous works have shown that both of them present a very good corrosion resistance in chloride contaminated media, between mortars as much as simulated pore solutions [12, 13]. However, the use of SS rebars has been limited due to their high cost compared to traditional carbon steel. Nickel is one of the alloying elements that significantly increase the cost of austenitic SSs. Its price has risen by 79% in the last five years, reaching a historic high of about 38,000 €/t in 2007 [14]. For this reason, new SSs, in which the nickel content is partly replaced by other elements, are being evaluated as possible alternatives to traditional carbon steel. Low-nickel austenitic SSs exhibit attractive properties, comparable to those of conventional austenitic SSs, such as good corrosion resistance, high strength and ductility, and a low tendency towards grain sensitization [15].

Despite the great advance in the field of SSs throughout the past years, electrochemical techniques still represent an effective tool that offer the possibility of studding the corrosion behavior in all different metals and passive alloys. Electrochemical techniques are effective accelerated laboratory tests that present the advantage of being highly sensitivity, easy to perform and reproduce, fast in data acquisition and, finally, easily comprehensible to interpret. Potentiodynamic polarization tests as well as electrochemical impedance spectroscopy (EIS), which has emerged as a powerful non-disturbing technique to study the passive films formed on the steel surface [16-18],

represent an excellent approach to study the corrosion behavior of metals and passive alloys, such as SSs, in a certain electrolyte, what is directly related to corrosion.

The aim of this work is to study the corrosion behavior of a new low–nickel SS in a carbonated calcium hydroxide ($Ca(OH)_2$) solution where the effect of chloride ions was investigated by polluting it with different amounts of sodium chloride (NaCl). This way, the effect of carbonation process on the passivity of the reinforcement, as well as the highly aggressive environment resulting from the dual effect of carbonation and the presence of chloride ions, are investigated. Conventional AISI 304 SS is also studied for comparative purposes, being the most common austenitic SS used as reinforcement.

2 MATERIALS AND METHODS

The test specimens consisted of 5.0 cm × 2.0 cm × 1.0 mm (Width × Length × Thickness) plates of the low-nickel austenitic SS and the AISI 304 SS. The decision to use plates instead of traditional bars was due to the design of the electrochemical cell.

The low-nickel and the AISI 304 SS samples were supplied by ACERINOX SA (Palmones, Cádiz, Spain). Table 1 shows the chemical composition (% by weight) of the two materials, according to the manufacturer. Specimens were initially ground using a series of silicon carbide (SiC) emery papers down to grade 600 before finishing with an ultrasonic clean in ethanol for one minute and rinsed with distilled water.

The test solution was a carbonated solution with different concentrations of chloride. A saturated $Ca(OH)_2$ solution with a pH~12–13 was prepared. Carbonation was achieved by bubbling CO_2 into the solution until a pH=8 was reached, a level below the referenced value of 9 to ensure the complete carbonation of the solution. The pH decrease

was controlled using a pHmeter (Crison GLP22). The precipitated $CaCO_3$ formed was filtered and different amounts of NaCl were added to the solution. The solution was used immediately after preparation to avoid contamination. The molar concentration of chloride in the solution was 0, 0.07, 0.17, 0.34, 0.51 and 0.85 M. The reason of using these molar concentrations is that they correspond to the following NaCl concentrations in weight percentage (wt. %): 0, 0.4, 1.0, 2.0, 3.0 and 5.0 %, which are very often used in corrosion science literature. In the present paper all concentrations are expressed in molarity.

The chemical products used to prepare the solutions were laboratory grade reagents: NaCl purisimum CODEX supplied by Panreac and $Ca(OH)_2$ for analysis supplied by Merck. All the solutions were prepared with distilled water.

One of the most common problems observed after a pitting resistance evaluation of a passive metal or alloy, as is the case of SS, throughout electrochemical methods is the presence of crevice corrosion. The occurrence of this type of corrosion, simultaneous to pitting corrosion, enables other corrosion mechanism, thus complicating the evaluation of the electrochemical behavior of the metallic material in the presence of pitting corrosion mechanisms only.

In order to minimize the effect of crevice corrosion, an *Avesta* cell was used [19] for the determination of the pitting potential (E_{pit}) by means of polarization curves measurements. The *Avesta* cell working procedure is based in the elimination of the aggressive solution contained in the crevice through the incorporation of distilled water in it. The aim of this method is not to eliminate the crevice, but to prevent the accumulation of aggressive ions and the local acidification in the crevice by the dilution of the solution contained within. With the aid of this particular type of electrochemical cell the E_{pit} is accurately determined.

A conventional three-electrode configuration was used, with the sample acting as working electrode, a saturated calomel electrode (SCE) as reference electrode and a platinum mesh as counter electrode. All the potentials presented in the present study are thus referred to the SCE.

A PARC 273A potentiostat (EG&G Instruments) was used to perform the electrochemical experiments. The corrosion potential (E_{corr}) of the samples was monitored for 40 min in each test solution. This was the time needed to reach a stable potential.

Pitting corrosion susceptibility was characterized by means of cyclic polarization curves. A potential scan rate of 0.1667 mV s^{-1} was used [20]. The current density limit for reversing the potential scan was 10^{-3} A cm^{-2}. The E_{pit} was defined as the potential value at which the current density sharply rises and the protection potential (E_{prot}) as the potential value at which the curve, in its reverse scan, intersects the passivity plateau.

EIS measurements were recorded at the E_{corr} in a frequency range from 10^5 Hz to 10^{-3} Hz with a logarithmic sweeping frequency of 5 points per decade. The EIS method involved the imposition of a 10 mV r.m.s. amplitude excitation voltage. A 1255A Solartron Frequency Response Analyser linked to an EG&G PARC 273A potentiostat was used for EIS measurements. Fitting of all the spectra were performed with Z–View software. All the experiments were performed at the room temperature of the laboratory (~25 ºC) and in triplicate to ensure reproducibility.

3 RESULTS AND DISCUSSION

3.1 Potentiodynamic Measurements

Fig. 1 shows the cyclic polarization curves for the low-nickel SS and the AISI 304 SS (for comparative purposes) in carbonated solution subjected to different chloride

concentrations. The E_{corr} values presented were very similar, though a small increase was observed as the chloride concentration increased in the solution. This small increase may indicate that a more stable film was formed on the metal surface but the increment is so small that should be taken carefully as it could also be due to very small surface differences after the sample preparation. A passivation–like behavior in a wide range of anodic potentials is observed by means of the plateaus of current densities exhibited in the curves.

The current density required to maintain a metal in a passive state is called passive current density (i_p) and represents a measure of the protectiveness of the film. At i_p the metal dissolution occurs at a nearly constant rate and the passive film formed on the metal surface grows thicker. Hence, a lower i_p is a consequence of a more corrosion resistant metal/alloy. As the potential in the metal tends to more anodic values, the current increases until a sharp rise can be observed normally due to the localized breakdown of the passivating oxide film. This breakdown causes the underlying metal dissolution leading to the formation of pits. Fig. 2 shows the current density dependence with potential in the passive region for the low-nickel SS and the AISI 304 SS. As observed in Fig. 2 for the low-nickel SS, in general meanings, the i_p increases as the chloride concentration grows in the solution indicating a lower corrosion resistance with the content of these ions. In a closer inspection, a threshold is found for chloride concentrations higher than 0.17 M with a noticeable increase in the current density. Above this concentration a less protective film is formed and the chlorides induce a higher dissolution of the SS. For the AISI 304 SS, although the overall trend observed is similar to the low-nickel SS with higher current densities as the chloride concentration increases, it is hard to determine a threshold only by the observation of the i_p. Nevertheless, above chloride concentrations of 0.17 M a sharp increase in the current density is exhibited at

lower potential values as the result of a lower resistance to pitting corrosion, as shown further on. It is interesting to remark that both SSs present i_p values of the same order, revealing their similar behavior in the passive region in terms of metal dissolution in carbonated solution under the effect of chlorides. This behavior is most likely due to a high similitude in the oxide films formed on both SSs.

The E_{pit} determines the local breakdown of the passive film, leading to an active corrosion state. In the absence of chloride, an E_{pit} of 0.563 V is observed for the low-nickel SS after a wide passivity plateau of ~480 mV (see Fig. 1a). When the chloride concentration is equal to 0.07 M, E_{pit} decreases in ~200 mV. The same trend is observed for the rest of chloride containing solutions, exhibiting a descent in the E_{pit} as the chloride ions increase. These results showed the directly proportional relationship between the tendency to localized corrosion and the concentration of chlorides in the carbonated solution. It is worth noting the fact that an E_{pit} is exhibited in the absence of chlorides, which can somewhat result unexpected as no halide is present in the solution. As previously mentioned, all the experiments were carried out in triplicate obtaining reproducible results with a defined E_{pit} for all of them. Thus, any accidental contamination with chlorides in the electrochemical cell is highly unlikely (neither being the source the synthetic electrolyte nor a leakage or flow of chlorides from the reference electrode solution to the test solution). Hence, the carbonate ions (CO_3^{2-}) appear to be responsible for this behavior. As previously reported [21], CO_3^{2-} is capable of causing pitting corrosion in AISI 304L SS and AISI 316L SS. The increase in the CO_3^{2-} concentration decreases the E_{pit} to more negative values, hence increasing the pitting corrosion susceptibility. According to this, the pits generated in the absence of chlorides in the present research work are attributed to the local breakdown of the passive films of the

low-nickel and the AISI 304 SSs as a consequence of the carbonates present in the test solution.

It is generally accepted after experimental observation over the last decades that for a given material E_{pit} in the presence of a halide (i.e. chloride ion) is a function of the halide activity as yielded in the following equation [22]:

$$E_{pit} = A - B \log a_{x^-} \quad (1)$$

where A and B are constants and a_{x^-} is the activity of the halogen anion. Taking the activity of chloride as unity, this relationship enables the estimation of E_{pit} for a given chloride concentration. As proposed by Macdonald [23], the Point Defect Model (PDM) accounts for the growth and breakdown of a passive film involving transport of anions (oxygen ion) and cations (metal ion) or their respective vacancies. Anions diffuse from the film/solution (f/s) interface to the metal/film interface (m/f) and subsequently resulting in the film thickening. Cations diffusion may results in breakdown of the passive film when metal vacancies (or metal holes) production rate at the f/s interface is higher than the rate of metal hole submergence into the bulk metal or alloy at the m/f interface. Under this assumption, cation vacancies pile up at the m/f interface and their accumulation above a critical value may act as a pit incubation process. When the halide is chloride the PDM yields the following relationship [24]:

$$E_{pit} = \frac{4.606\,RT}{xF\alpha} \log \frac{J_m}{J^0 u^{-x/2}} - \frac{2.303\,RT}{\alpha F} \log a_{Cl^-} \quad (2)$$

where J_m is the rate of submergence of metal holes into the metal, x is the charge on a cation, J^o *a*nd u are exponential terms related to the metal and oxygen vacancies in the film (more information about this term can be found in Ref. [24]), α is a parameter that indicates the external potential dependency of the potential drop across the m/f interface

and F, R and T have their usual meanings. The form of Eq. (2) coincides with the experimental Eq. (1), where

$$A = \frac{4.606\,RT}{xF\alpha} \log \frac{J_m}{J^0 u^{-x/2}} \tag{3}$$

and

$$B = \frac{2.303\,RT}{\alpha F} \tag{4}$$

Fig. 3 shows the linearity between E_{pit} and log[Cl^-] for the low-nickel SS. The values of A and B parameters can be obtained from this plot, resulting in A = 224.98 mV and B = 114.64 mV. The parameter α can be calculated then from $\alpha = 2.303RT/BF$ yielding an experimental value of 0.516 for the low-nickel SS at 25 ºC. Similar experimental B values were obtained by Strehblow and Titze for iron in borate buffer solution (pH = 8) [25] and by Yashiro *et al*. for AISI 304 SS when they studied the E_{pit} dependence with temperature in chloride containing solutions [22]. As observed in the inset in Fig. 3, values of A and B for the AISI 304 SS could not be determined since no linear-like behavior of the E_{pit} vs. log [Cl^-] was detected. This may be due to differences in the experimental setup with respect to the bibliographic data presented as the *Avesta* cell was used. Nevertheless, important information is deduced from the variation of the E_{pit} with the applied voltage depicted in Fig. 3 (see inset). The AISI 304 SS shows higher E_{pit} values than the low-nickel SS for all the chloride concentrations used. The bigger differences are observed in the absence of chlorides and when the minimum chloride concentration is present. The increase in the E_{pit} for the AISI 304 in the absence of chlorides informs about the lower tendency to localized corrosion due to the effect of carbonate ions. When a concentration of 0.07 M of chloride ions is added, the combination of the carbonate and chloride anions creates a double effect on the oxide film of both SSs, being the one formed on the low-nickel SS less resistant than that on the AISI 304 SS when high overpotentials

are applied. With the increase of [Cl^-], the low-nickel SS presents a linear decay in its E_{pit} while the AISI 304 SS exhibits a stable value of approximately 375 mV_{SCE}. Thus, of chlorides present an important role on the film stability and this could be explained in terms of the passive layer thickness as it will be discussed in detail later on.

After the current density limit imposed was reached, all the potentiodynamic tests defined an E_{prot}, after a clear hysteresis loop. The E_{prot} is the potential at which a stable growing pit ceases to grow and below which repassivation of existing pits is achieved. Although it occurrence has been widely observed, the use of E_{prot} is still controversial on the basis of the following arguments [26]: (i) the measured E_{prot} is inversely dependent on the pit depth and, because of this, the E_{prot} measured in shallow pits or by a relatively rapid scan rate may not be sufficiently conservative, and (ii) the E_{prot} measured on deep pits may be too low and therefore unnecessarily conservative for predicting the occurrence of localized corrosion. Predictive models have been proposed to explain and calculate the E_{prot} as a function of environmental conditions. Okada proposed that the steps taking place in repassivation are as follow: a thin oxide film forms on the metal surface which, in contact with the non-protective metal halide (i.e. chloride) film, is strongly corroding at the pit bottom, then the oxide extends over the active area of the pit resulting in a passive film that prevents the dissolution of the metal base [27]. A linear dependence of E_{prot} on the activity of the halide was observed in an analogous way than that presented previously for E_{pit}. However, this model presented deficiencies when reproducing the two distinct slopes of the E_{prot} dependence on the logarithm of the activity of chlorides observed for very low activity values as well as explaining the drastic changes in E_{prot} in a corrosion inhibited environment. To account for these limitations, Anderko *et al*. [26], inspired by the work of Okada [27], developed a model based in competitive reaction of various species leading to the formation of oxide within a metal

salt film for predicting E_{prot} on different passive alloy/environment systems. They also found that for a number of corrosion resistant alloys, the repassivation potential has a complex dependence on the logarithm of chloride concentration [26].

The variation of E_{prot} for the low-nickel SS as a function on the logarithm of chloride concentration is shown in Fig. 4. It is observed that a linear-like behavior was exhibited as predicted by the models previously described [26, 27]. A decrease of E_{prot} with increasing chloride was exhibited, indicating a more difficult repassivation of the generated pits. Only a single logarithmic slope was observed in the curves depicted in Fig. 4 because the chloride concentration did not reach a sufficiently low value, as has been generally reported for AISI 304 SS in chloride containing solutions [26]. This behavior is determined by the parameters that represent the dissolution of the metal through the formation of metal/chloride complexes [26]. Fig. 4 also shows the E_{corr} values presented by the low-nickel SS and the AISI 304 SS in the carbonated solution subjected to different chloride concentrations. As observed, the increase in [Cl^-] resulted in a progressive approach of the E_{prot} to the E_{corr}, reducing the region where repassivation is achieved and making the materials less corrosion resistant. Despite this fact, repassivation was accomplished for all chloride concentrations used.

3.2 Electrochemical Impedance Spectroscopy (EIS)

Bode plots for the low-nickel SS and the AISI 304 SS in carbonated solution subjected to different chloride concentrations are shown in Figs. 5 and 6, respectively. These comparative measurements show that both SSs exhibited a similar behaviour with changes in log|Z| and phase angle vs. log(f). In these plots f is the frequency and |Z| the impedance modulus. At high frequencies the impedance modulus defined a straight line with a zero slope and the phase angle remained in zero degrees, indicating a resistive-like

behavior not associated to a relaxation process. This resistance was attributed, as commonly accepted, to the electrolyte resistance. Bode plots showed a capacitive-like behavior at the medium and low frequencies, characterized by a slanted impedance modulus and a phase angle defined maximum. When the lowest frequencies were reached the phase angle tended to zero as the impedance modulus approached a resistance. Thus, from the raw observation of the experimental data the system appeared to be defined by a single relaxation process. Additionally, the phase angle maximum smaller than 90º (~75º) and the absolute value of the impedance modulus slope lower than unity (~0.8) suggest a deviation from the ideal capacitor, generally due to dispersion of the time constant caused by irregularities on the electrode surface, surface roughness, fractal surface and, in general, processes associated with an irregular distribution of the applied potential [28].

Before proceeding to the evaluation of the impedance data, the Kramers–Kronig transforms (KK) were used with the aim of evaluating the consistency of EIS experimental data [29]. General KK relations are integral equations with real and imaginary parts as given in Eqs. (5–7).

$$Z'(\omega) = Z'(\infty) + \frac{2}{\pi}\int_0^\infty \frac{xZ''(x) - \omega Z''(\omega)}{x^2 - \omega^2} dx \quad (5)$$

$$Z'(\omega) = Z'(0) + \frac{2}{\pi}\int_0^\infty \frac{(\omega/x)Z''(x) - Z''(\omega)}{x^2 - \omega^2} dx \quad (6)$$

$$Z''(\omega) = -\frac{2\omega}{\pi}\int_0^\infty \frac{Z'(x) - Z'(\omega)}{x^2 - \omega^2} dx \quad (7)$$

where Z'(x) and Z''(x) are the real (Z_{real}) and imaginary (Z_{imag}) parts of the impedance, respectively; x ($0<x<\infty$) is the integration variable and ω is the angular frequency. Using Eqs. (5) and (6) it is possible to transform the imaginary part into the real part and *vice*

versa, Eq. (7). Comparison of the experimental plots with the transformed plots by means of KK transforms represents a validation test for EIS measurements.

Figs. 7 and 8 show the comparison between the EIS experimental data and those obtained by means of the KK transforms for the low–nickel SS and the AISI 304 SS in carbonated solution subjected to a chloride concentration equal to 0.51 M, respectively. Only Figs. 7 and 8 are presented due to its representative nature as both SSs exhibited very similar diagrams in all the range of chloride concentration used. A good consistency of the experimental data was observed, existing a small dispersion at very low frequency values for both SSs (lower than 4×10^{-2} Hz) probably due to a lack of stability in the relaxation processes experienced by the system in such frequencies or the presence of noise during the measurement.

Additionally, the results were analysed by comparing the transformed data with the experimental data, using a statistical error function [30]:

$$\Delta\overline{Z} = \frac{100\sum_{x=1}^{N}\left|Z_{\exp}(x) - Z_{KK}(x)\right|}{NZ_{\max}} \tag{8}$$

where $\left|Z_{\exp}(x) - Z_{KK}(x)\right|$ represents the absolute magnitude of the difference between the value of the experimental impedance ($Z_{\exp}(x)$) and that calculated via the KK transform, ($Z_{KK}(x)$); $Z_{\max}$ is the maximum value of the experimental impedance, and N the number of points in the experimental data.

Table 2 shows the average error, $\Delta\overline{Z}$ (%), obtained using Eq. (8) for both SSs. It is observed that the calculated average errors were always lower or equal to 2.74%, both the real to imaginary and the imaginary to real transformation. The fact that these errors were always lower than 3.0% confirms the consistency and therefore, the validity of the experimental data obtained by means of EIS, as the KK transforms were satisfied [30].

Impedance data were fitted using the electrical equivalent circuit (EEC) depicted in Fig. 9. A constant phase element (CPE) unit was used to account for the frequency dispersion observed. This EEC consisted of a resistance, R_e, in series with a parallel combination of a CPE unit and a second resistance, R_p. For the lowest frequency values, the phase angle tended to zero reporting no evidence of corrosion, normally characterized by the presence of diffusion processes in the low frequency domain. In addition, no apparent sign of pits was found after the EIS measurements, so that a passive-like behavior was assumed to be exhibited by the system in the test conditions. This is in agreement with the low current density values shown in the proximity of the E_{corr} (see Fig. 1). Consequently, the time constant (τ) presented at medium and low frequency values was associated to the electric resistance of the passive film to the current flow, where R_p was the polarization resistance; and the CPE unit represents the capacitance associated to the system, which will be discussed in detail later on. Finally, R_e represents the electrolyte resistance between the reference electrode and the working electrode.

A CPE is often used instead of an ideal capacitor to account for the non-ideal capacitance of the electrode. The impedance of a CPE is defined by the expression:

$$Z_{CPE} = \frac{1}{Y_0 (j\omega)^n} \tag{9}$$

where Y_0 is the admittance, $j^2 = (-1)$, ω is the angular frequency, and n is a dimensionless fractional exponent. When n equals 1 a CPE simplifies to a capacitor; when n equals 0 a CPE represents a pure resistor, and when n equals 0.5 a CPE behaves as a Warburg impedance.

The EEC proposed in the present work, previously reported by El–Egamy and Badaway [31] to account for the passivity and passivity breakdown of the AISI 304 SS in alkaline solutions, was selected as it provided a good fitting of the experimental results and represented a good description of the electrochemical system keeping the number of

circuit elements at a minimum. Figs. 5 and 6 also show the fitting results, exhibiting an excellent concordance with the experimental data. At very high frequencies (10^4–10^5 Hz) the phase angle plot showed positive values since the imaginary part of the impedance appeared below the real axis. This is most likely due to the inductance associated to the wires connecting the electrochemical cell and the potentiostat. These artifacts present in the experimental data were discarded in the analysis since they do not correspond to any physical process in the studied system.

The total impedance of the model proposed presents the following transfer function:

$$Z = R_e + \frac{R_p}{1 + Y_0 R_p (j\omega)^n} \tag{10}$$

where all the parameters have the meaning previously described. Table 3 reports the fitting result of the experimental impedance data for the low-nickel SS and for the AISI 304 SS in carbonated solution subjected to different chloride concentrations yielded using the EEC of Fig. 9.

It is worth noting that the plot of the phase angle vs. log(*f*) presented in Figs. 5 and 6 may suggest the presence of more than one time constant with the increase of chloride concentration. With the aim of determine such a case additional EEC models were evaluated. The association of two time constants, either in parallel or in series [18, 32], has been so far the most often proposed model; whereas the physical interpretation of the circuit elements is not always clear and remains nowadays subjected to a big controversy. These two time constant EEC's were evaluated but the simulation errors where significantly higher resulting in a not suitable models to interpret the systems presented in the present work.

Upon closer inspection of the data, R_e appeared to be responsible for the phase angle shifting and broadening. The phase angle is defined by $\phi = \arctan(Z''/Z')$, where ϕ represents the phase angle and, Z'' and Z' are the imaginary and real part of the impedance when expressed as a complex number, respectively. Being R_e contained exclusively in the real part of the impedance transfer function, an influence of this parameter on the phase angle plot is expected. Considering an electrochemical system controlled by a single relaxation process, when R_e increases the high frequency limit of the real part of the impedance becomes higher, shifting the phase angle peak towards lower frequency values and reducing the capacitive region. Consequently, a broadening of the phase angle plot and a shift of its maximum is observed when R_e decreases, thus increasing the capacitive region. This is in perfect agreement with the results presented in Figs. 5 and 6, where the phase angle exhibited a broadening and its maximum shifted to higher frequency values with the increase in the chloride concentration, showing a larger capacitive region in the frequency domain.

As previously described, the impedance of a CPE unit is dependent on the fractional exponent n, which in the case of a pure capacitor is equal to unity. In such a case, the admittance of the system results in the capacitance's analog. Nevertheless, when n deviates from unity, even if that deviation is small, the approximation of Y_0 to a capacitance should be avoided as it may result in large computational errors [33]. In order to evaluate the evolution of the capacitance with respect to [Cl^-], the effective capacitance (C_{eff}) of the different systems under study was calculated. Hsu and Mansfeld equation, Eq. (11), suggests that C_{eff} can be calculated from Y_0 upon the observation that the maximum in the imaginary component of the impedance occurs at the same critical frequency (ω_c), regardless of the value of α [34].

$$C_{eff} = Y_0(\omega_c)^{\alpha-1} \tag{11}$$

where ω_c is the critical angular frequency (rad/s). The critical frequency, defined as the point where the maximum in the imaginary component of the impedance occurs, represents an important parameter since in the case of an ideal capacitor it allows the determination of the capacitance associated to a particular relaxation process defined by a Voigt element according to the following expression: $C = 1/\omega_c R$. In the case of a CPE unit, ω_c can be calculated from values of Y_0, R_p and α found from the fitting results of the experimental impedance data according to the following expression [34]:

$$\omega_c = \left(\frac{1}{R_p Y_0} \right)^{1/\alpha} \tag{12}$$

Using Eq. (12), the critical frequency was found to be 7 mHz for the low-nickel SS and 6 mHz for AISI 304 SS (from 0 M to 0.85 M). Thus, in the present work none of the SSs studied presented a critical frequency below the experimentally measured frequency, indicating that the passive films did not change during the EIS measurements conducted at the low value of the critical frequency. Fig. 10 shows the deviation of the Y_0 with respect to C_{eff}, calculated using Eq. (11). A remarkable difference is observed between these two parameters, confirming the unsuitability of the use of the admittance as a capacitance value for the study of an electrical double layer, even for an α value close to unity.

As commonly accepted, the system formed by a SS in contact with an electrolyte is constituted by the metal base covered by a thin layer of an oxide that presents semiconducting properties in direct contact with the electrolyte. This general structure establishes three different capacitances: (i) a first capacitance associated to the m/f interface due to the charge alignment resulting from the difference of the Fermi level on each side (C_M), (ii) a second capacitance associated to the f/s interface normally explained by means of the Helmholtz double layer (C_H) and, (iii) a third capacitance associated to

the passive film due to the space charge layer generated inside the film (C_{SC}) [35]. The combination of these three series capacitances results in the total capacitance of the system (C_T), expressed by the following equation:

$$\frac{1}{C_T} = \frac{1}{C_M} + \frac{1}{C_{SC}} + \frac{1}{C_H} \tag{13}$$

Being the charge carrier density in metals much higher than in semiconductors, it is reasonable to assume that C_M is larger than C_{SC}. Additionally, it is well known that the capacitance associated to the Helmholtz double-layer is bigger than C_{SC} [35]. Consequently, C_M and C_{SC} are negligible according to Eq. (13) and C_T is approximately equal to C_{SC}. According to this, the C_{eff} obtained by the impedance measurements, which in this particular system is the C_T analog, was considered as a global capacitance associated to the passive film.

A closer inspection of C_{eff} for the low-nickel SS and AISI 304 SS with respect to [Cl^-] is shown in Fig. 11, where the same trend was observed for both SSs. A linear-like behavior was exhibited with bigger C_{eff} values when the chloride concentration increased. As observed, both materials accomplished a similar slope. The calculated C_{eff} values range from 67 to 90 μF cm^{-2} for the low-nickel SS and from 78 to 97 μF cm^{-2} for AISI 304 SS, as shown in Fig. 11. For both SSs the minimum capacitances were observed in the absence of chloride. As the chloride concentration grows in the solution an increase in C_{eff} values is observed. As shown in Fig. 11, the calculated capacitances were very similar, being for the low-nickel SS always slightly lower than those observed for AISI 304, with a difference of ~10 μF cm^{-2} both in the absence and presence of chloride in the solution.

The thicknesses (δ) of the passive films formed were estimated from C_{eff} capacitance values assuming the model of a parallel plate capacitor defined by the following expression:

$$\delta = \frac{\varepsilon_0 \varepsilon}{C_{eff}} \tag{14}$$

where ε_o was the vacuum permittivity (8.854×10^{-12} F m^{-1}) and ε was the dielectric constant of the passive film formed on SS, ε= 15.6 [36]. It is well known that, along with chemical composition, the thickness of a passive layer plays a significant role in the corrosion resistance of a metal or a passive alloy. For similar chemical composition, a thicker layer provides a more effective barrier against corrosive agents. Thus, changes in the passive film thickness of the oxide films formed on the SSs studied is extremely informative. As shown in Fig. 12 a negative linear relationship was found between the δ of the passive films formed on both the low-nickel and the AISI 304 SSs and [Cl^-], indicating that the amount of chloride in the electrolyte resulted in a thinner and thus less protective passive layer. This finding is supported by a previous work where the thickness of the oxide layer formed on the low-nickel SS studied in the present paper and the AISI 304 SS were inversely related to the chloride concentration in the electrolytic media [37]. As observed in Fig. 12, the low-nickel SS appears to present thicker passive films than the AISI 304 SS both in the absence and presence of chloride ions. This may suggest a higher corrosion resistance. Nevertheless, these differences are of the order of 10^{-2} nm and may be due error accumulation during the C_{eff} calculation or to small deviations in their oxide layer chemistry that, although of a very similar nature [37] is not precisely equal. Thus, based on the results obtained it is observed that both SSs present comparable passive film thicknesses and, consequently, an equivalent corrosion resistance in the test solutions used in the present work under non polarization conditions.

As previously indicated, R_p represents the electric resistance of the passive film to the current flow. The electric resistance of a conductor is expressed as follows:

$$R = \frac{\rho L}{A} \tag{15}$$

where R is the electric resistance (Ω), ρ is the electrical resistivity of the conductor (Ω cm), A is the cross-section area (cm^2) and L is the length (cm), which in the case of a passive film is the thickness analog. Consequently, under a comparable chemical composition, differences in R_p indicate changes in the oxide layer thickness. As observed in Table 3, when the chloride concentration increased in the solution, a monotonous decrease in the R_p values is observed, indicating a progressively lower corrosion resistance for both SSs. It is interesting to remark how the effect of carbonation processes, by itself, reduces significantly the corrosion resistance of the low-nickel SS, exhibiting a R_p value in carbonated solution in the absence of chloride lower than the one observed in a previous work [14], where the same material was exposed to a fresh non-carbonated solution of saturated $Ca(OH)_2$ with a chloride concentration equal to 0.85 M. As observed, the low-nickel SS present almost identical R_p values than the conventional AISI 304 SS in the chloride concentration range (see Table 3). This finding is supported by all the experimental results previously presented in this paper and confirm that the presence of chlorides does not only affect the corrosion resistance when an overpotential is applied on the system (Figs. 2 and 3) but also affects the protective properties of the passive layer in the non-polarized state.

3.3 Corrosion Current Density (i_{corr})

It may be assumed, as an approximation, that the polarization resistance (R_p) is inversely proportional to the current density at the E_{corr}, also referred as corrosion current density (i_{corr}), which is directly related to the corrosion rate of a corrosion process [38]. Thus, the determination of i_{corr} provides important information about the kinetics of the corrosion process as well as the corrosion resistance of a metal or an alloy in a particular

environment. Impedance fitting results were used to calculate i_{corr} by means of the Stern−Geary equation:

$$i_{corr} = \frac{B}{R_p} \tag{16}$$

where B is a constant determined by the Tafel slopes according to the following expression:

$$B = \frac{\beta_a |\beta_c|}{2.303(\beta_a + |\beta_c|)} \tag{17}$$

where β_a and β_c are the anodic and the cathodic Tafel slopes, respectively. Due to the novelty of the low-nickel SS studied in the present work and the specific character of this parameter for each particular system [39], β_a and β_c were experimentally determined for both SSs. For this purpose, a pontentiodynamic polarization of 250 mV was performed both in the cathodic and in the anodic direction from the E_{corr} for the low-nickel SS and the AISI 304 SS in each particular solution, where the Tafel slopes were calculated after the linear fit of the Tafel region (see Fig. 13 which is presented as a representative example of the procedure). Table 4 shows the Tafel slopes and the experimental B constant calculated for the low-nickel SS (B~53 mV/decade) and the AISI 304 SS (B~48 mV/decade) in carbonated solution subjected to different chloride concentrations. As observed in Table 4, the low-nickel SS presented bigger B constant values than the AISI 304 SS resulting from more slanted anodic and cathodic slopes. Once the B constant was determined, i_{corr} values were calculated using Eq. (16), where R_p represents the ~~R_{ct}~~ the polarization resistance obtained by the experimental impedance data analysis. In addition, i_{corr} values were determined by means of the direct current (DC) measurements from the point of intersection of the Tafel plots at the E_{corr}.

Fig. 14 shows the comparative i_{corr} values for both SSs, the low-nickel and the AISI 304, in carbonated solution subjected to different chloride concentrations obtained by DC and AC measurements. A good agreement is found between both methods with the bigger differences in the absence of chlorides and for the lowest chloride concentration of approximately 0.03 to 0.06 μF cm^{-2}, which can be consider a negligible dispersion. As observed, both SSs exhibit the same trend since i_{corr} increases linearly with the increase in [Cl^-], indicating a less corrosion resistance as the halide concentration grows in the solution. Nevertheless, the i_{corr} values, always of the order of 10^{-7} μF cm^{-2}, confirm that the systems exhibit a passive-like behavior in the proximity of the E_{corr}. As observed, the low-nickel SS shows similar i_{corr} values to the AISI 304 SS in the presence of chlorides, indicating a comparable corrosion resistance in the non-polarized state under the experimental conditions, and supporting the results previously presented in this study.

4 CONCLUSIONS

Electrochemical tests have been performed on a new low-nickel SS in a carbonated $Ca(OH)_2$ solution subjected to different chloride concentrations. The effect of carbonation process as well as the combined effect of carbonation and the presence of chloride was studied. Potentiodynamic tests show that the E_{corr} slightly tended towards more noble values, while the E_{pit} decreased, as the chloride concentration increased in the carbonated solution. In terms of passivity, low-nickel SS showed a passive-like behaviour in all the chloride concentrations studied with defined passivity plateaus, although a descent was observed as the chloride concentration increased. EIS results showed that R_p values decreased with the addition of chloride. Calculated thickness exhibited a linear–like behaviour tending towards thinner passive films as chloride concentration increased. Determined i_{corr} values grown with [Cl^-]. The effect of carbonation, by itself, affected the

corrosion resistance of the low-nickel SS in a detrimental way; whereas, the combined effect of carbonation and chloride ions increased the corrosion susceptibility leading to a lower corrosion resistance. In comparison with the traditional AISI 304 SS, the low-nickel SS presented very similar corrosion behaviour to the conventional AISI 304 SS.

ACKNOWLEDGEMENTS

M. Criado expresses her gratitude to the Spanish Research Council (CSIC) for their contract under the Juan de la Cierva Program founded by the Spanish Ministry of Economy and Competitiveness. D.M. Bastidas gratefully acknowledges funding from the Ramón and Cajal Program founded by the Spanish Ministry of Economy and Competitiveness. The authors express their gratitude to Project BIA2008-05398 from CICYT, Spain, for financial support and to ACERINOX SA for supplying the studied low-nickel and AISI 304 stainless steels.

REFERENCES

[1] L. Freire, M.J. Carmezim, M.G.S. Ferreira, M.F. Montemor, The electrochemical behaviour of stainless steel AISI 304 in alkaline solutions with different pH in the presence of chlorides, Electrochim. Acta, 56 (2011) 5280-5289.

[2] A. Bautista, G. Blanco, F. Velasco, Corrosion behaviour of low-nickel austenitic stainless steels reinforcements: A comparative study in simulated pore solutions, Cement and Concrete Res. 36 (2006) 1922-1930.

[3] E.E. Rees, D.S. McPhail, M.P. Ryan, J. Kelly, M.G. Dowsett, Low energy SIMS characterisation of ultra thin oxides on ferrous alloys, Appl. Surf. Sci. 203-204 (2003) 660-664.

[4] W. Chen, R.-G. Du, C.-Q. Ye, Y.-F. Zhu, C.-J. Lin, Study on the corrosion behavior of reinforcing steel in simulated concrete pore solutions using in situ Raman spectroscopy assisted by electrochemical techniques, Electrochim. Acta 55 (2010) 5677-5682.

[5] M.B. Valcarce, M. Vázquez, Carbon steel passivity examined in alkaline solutions: The effect of chloride and nitrite ions, Electrochim. Acta 53 (2008) 5007-5015.

[6] R. Montoya, W. Aperador, D.M. Bastidas, Influence of conductivity on cathodic protection of reinforced alkali-activated slag mortar using the finite element method, Corros. Sci. 51 (2009) 2857-2862.

[7] Z.Q. Tan, C.M. Hansson, Effect of surface condition on the initial corrosion of galvanized reinforcing steel embedded in concrete, Corros. Sci. 50 (2008) 2512-2522.

[8] N.R. Baddoo, Stainless steel in construction: A review of research, applications, challenges and opportunities, J. Constr. Steel Res. 64 (2008) 1199-1206.

[9] A. Bautista, G. Blanco, F. Velasco, M.A. Martı´nez, Corrosion performance of welded stainless steels reinforcements in simulated pore solutions, Constr. Build. Mater. 21 (2007) 1267-1276.

[10] L. Veleva, M.A. Alpuche-Aviles, M.K. Graves-Brook, D.O. Wipf, Voltammetry and surface analysis of AISI 316 stainless steel in chloride-containing simulated concrete pore environment, J. Electroanal. Chem. 578 (2005) 45-53.

[11] C.J. Abbot, Steel corrosion solution, Concr. Eng. Int. 3 (1999) 39-43.

[12] C.M. Abreu, M.J. Cristóbal, R. Losada, X.R. Nóvoa, G. Pena, M.C. Pérez, Comparative study of passive films of different stainless steels developed on alkaline medium, Electrochim. Acta 49 (2004) 3049-3056.

[13] L. Freire, M.J. Carmezim, M.G.S. Ferreira, M.F. Montemor, The passive behaviour of AISI 316 in alkaline media and the effect of pH: A combined electrochemical and analytical study, Electrochim. Acta 55 (2010) 6174-6181.

[14] S. Fajardo, D.M. Bastidas, M. Criado, M. Romero, J.M. Bastidas, Corrosion behaviour of a new low-nickel stainless steel in saturated calcium hydroxide solution, Constr. Build. Mater. 25 (2011) 4190-4196.

[15] A. Di Schino, M. Barteri, J.M. Kenny, Fatigue behavior of a high nitrogen austenitic stainless steel as a function of its grain size, J. Mater. Sci. Lett. 22 (2003) 1511-1513.

[16] D.M. Bastidas, Interpretation of impedance data for porous electrodes and diffusion processes, Corrosion 63 (2007) 515-521.

[17] M. Sánchez, J. Gregori, C. Alonso, J.J. García-Jareño, H. Takenouti, F. Vicente, Electrochemical impedance spectroscopy for studying passive layers on steel rebars immersed in alkaline solutions simulating concrete pores, Electrochim. Acta 52 (2007) 7634-7641.

[18] G. Blanco, A. Bautista, H. Takenouti, EIS study of passivation of austenitic and duplex stainless steels reinforcements in simulated pore solutions, Cement Concr. Compos. 28 (2006) 212-219.

[19] R. Ovarfort, New electrochemical cell for pitting corrosion testing, Corros. Sci. 28 (1988) 135-140.

[20] ASTM G61-86, Standard Test Method for Conducting Cyclic Potentiodynamic Polarization Measurements for Localized Corrosion Susceptibility of Iron-, Nickel-, or Cobalt-Based Alloys (2009).

[21] S.A.M. Refaey, F. Taha, A.M.A. El-Malak, Corrosion and inhibition of stainless steel pitting corrosion in alkaline medium and the effect of Cl− and Br− anions, Appl. Surf. Sci. 242 (2005) 114-120.

[22] H. Yashiro, K. Tanno, S. Koshiyama, K. Akashi, Critical Pitting Potentials for Type 304 Stainless Steel in High-Temperature Chloride Solutions, Corrosion 52 (1996) 109-114.

[23] D.D. Macdonald, The history of the Point Defect Model for the passive state: A brief review of film growth aspects, Electrochim. Acta 56 (2011) 1761-1772.

[24] L.F. Lin, C.Y. Chao, D.D. Macdonald, Point Defect Model for anidic passive films, J. Electrochem. Soc. 128 (1981) 1194-1198.

[25] H.H. Strehblow, B. Titze, Pitting potentials and inhibition potentials of iron and nickel for different aggressive and inhibiting anions, Corros. Sci. 17 (1977) 461-472.

[26] A. Anderko, N. Sridhar, D.S. Dunn, A general model for the repassivation potential as a function of multiple aqueous solution species, Corros. Sci. 46 (2004) 1583-1612.

[27] T. Okada, Considerations of the stability of pit repassivation during pitting corrosion of passive metals, J. Electrochem. Soc. 131 (1984) 1026-1032.

[28] V. Feliú, J.A. González, C. Andrade, S. Feliú, Equivalent circuit for modelling the steel-concrete interface. I. experimental evidence and theoretical predictions, Corros. Sci. 40 (1998) 975-993.

[29] D.D. Macdonald, Reflections on the history of electrochemical impedance spectroscopy, Electrochim. Acta 51 (2006) 1376-1388.

[30] J.R. Scully, D.C. Silverman, M.W. Kendig, Electrochemical impedance: analysis and interpretation, ASTM 1993.

[31] S.S. El-Egamy, W.A. Badaway, Passivity and passivity breakdown of 304 stainless steel in alkaline sodium sulphate solutions, J. Appl. Electrochem. 34 (2004) 1153-1158.

[32] C.M. Abreu, M.J. Cristóbal, R. Losada, X.R. Nóvoa, G. Pena, M.C. Pérez, Long-term behaviour of AISI 304L passive layer in chloride containing medium, Electrochim. Acta 51 (2006) 1881-1890.

[33] S.P. Harrington, F. Wang, T.M. Devine, The structure and electronic properties of passive and prepassive films of iron in borate buffer, Electrochim. Acta 55 (2010) 4092-4102.

[34] C.H. Hsu, F. Mansfeld, Technical Note: Concerning the Conversion of the Constant Phase Element Parameter Y_0 into a Capacitance, Corrosion 57 (2001) 747-748.

[35] E.M.A. Martini, I.L. Muller, Characterization of the film formed on iron in borate solution by electrochemical impedance spectroscopy, Corros. Sci. 42 (2000) 443-454.

[36] N.B. Hakiki, S. Boudin, B. Rondot, M. Da Cunha Belo, The electronic structure of passive films formed on stainless steels, Corros. Sci. 37 (1995) 1809-1822.

[37] S. Fajardo, D.M. Bastidas, M.P. Ryan, M. Criado, D.S. McPhail, R.J.H. Morris, J.M. Bastidas, Low energy SIMS characterization of passive oxide films formed on a low-nickel stainless steel in alkaline media, Appl. Surf. Sci. 288 (2014) 423-429.

[38] ASTM G102-89, Standard Practice for Calculation of Corrosion Rates and Related Information from Electrochemical Measurements, 2010.

[39] S. Feliu, J.A. González, J.M. Miranda, V. Feliu, Possibilities and problems of in situ techniques for measuring steel corrosion rates in large reinforced concrete structures, Corros. Sci. 47 (2005) 217-238.

Table 1. Chemical composition (wt.%) of the low-nickel SS and the AISI 304 SS studied. The balance was Fe.

Material	C	Si	Mn	P	S	Cr	Ni	Mo	Cu	N
Low-nickel	0.082	0.48	7.26	0.027	0.001	16.56	4.32	0.07	0.13	0.075
AISI 304	0.049	0.32	1.75	0.028	0.001	18.20	8.13	0.22	0.21	0.050

Table 2. Average error values, $\Delta\overline{Z}$ (%), for the low-nickel SS and the AISI 304 SS in carbonated solution (pH=8, 25 ºC) with different chloride concentrations.

$[Cl^-]$ (mol l^{-1})	$\Delta\overline{Z}$ (%)			
	Low-Nickel SS		AISI 304 SS	
	$Z_{Imag}\rightarrow Z_{Real}$	$Z_{Real}\rightarrow Z_{Imag}$	$Z_{Imag}\rightarrow Z_{Real}$	$Z_{Real}\rightarrow Z_{Imag}$
0	0.50	1.56	0.52	1.17
0.07	0.97	2.54	1.33	1.26

0.17	0.77	2.26	0.77	2.26
0.34	0.89	1.60	0.56	1.64
0.51	0.69	1.25	0.93	2.35
0.85	0.60	1.82	0.45	1.19

Table 3. Fitting results of EIS experimental data for the low-nickel SS and the AISI 304 SS in carbonated solution (pH=8, 25 ºC) subjected to different chloride concentration.

Low-Nickel SS									
$[Cl^-]$ (mol l^{-1})	R_e (Ωcm^2)	Error (%)	R_p ($M\Omega cm^2$)	Error (%)	Y_0 ($\mu Scm^{-2}s^n$)	Error (%)	n	Error (%)	χ^2
0	1005	0.41	0.204	0.77	50.01	0.51	0.89	0.25	3.1×10^{-3}
0.07	152	0.90	0.197	1.36	53.88	0.86	0.88	0.32	5.2×10^{-3}
0.17	83	0.94	0.188	1.36	54.78	0.84	0.88	0.28	4.5×10^{-3}
0.34	45	1.20	0.175	1.58	56.22	1.00	0.89	0.31	5.8×10^{-3}
0.51	29	1.06	0.171	1.15	58.98	0.71	0.89	0.20	2.6×10^{-3}
0.85	19	1.48	0.158	1.74	65.41	1.10	0.88	0.31	6.4×10^{-3}
AISI 304 SS									
0	977	0.78	0.217	0.98	55.54	0.55	0.88	0.17	1.6×10^{-3}
0.07	159	1.09	0.192	1.72	57.53	1.06	0.88	0.30	8.6×10^{-3}
0.17	85	1.05	0.187	1.49	58.08	0.90	0.87	0.34	4.8×10^{-3}
0.34	48	0.97	0.178	1.30	59.29	0.76	0.87	0.27	3.2×10^{-3}
0.51	28	0.73	0.171	0.95	63.89	0.56	0.88	0.16	1.8×10^{-3}
0.85	19	0.49	0.162	0.81	67.58	0.53	0.87	0.26	2.1×10^{-3}

Table 4. Tafel slopes, β_a and β_c, and B constant for the low-nickel SS and the AISI 304 SS in carbonated solution (pH=8, 25 ºC) with different chloride concentrations.

$[Cl^-]$ (mol l^{-1})	Low-Nickel			AISI 304		
	β_a (mV/decade)	β_c (mV/decade)	B (mV/decade)	β_a (mV/decade)	β_c (mV/decade)	B (mV/decade)
0	298	–212	54	263	–197	49
0.07	300	–209	53	275	–188	49
0.17	302	–199	52	273	–182	47
0.34	317	–199	53	277	–180	47
0.51	316	–195	52	292	–183	49
0.85	321	–194	53	278	–185	48

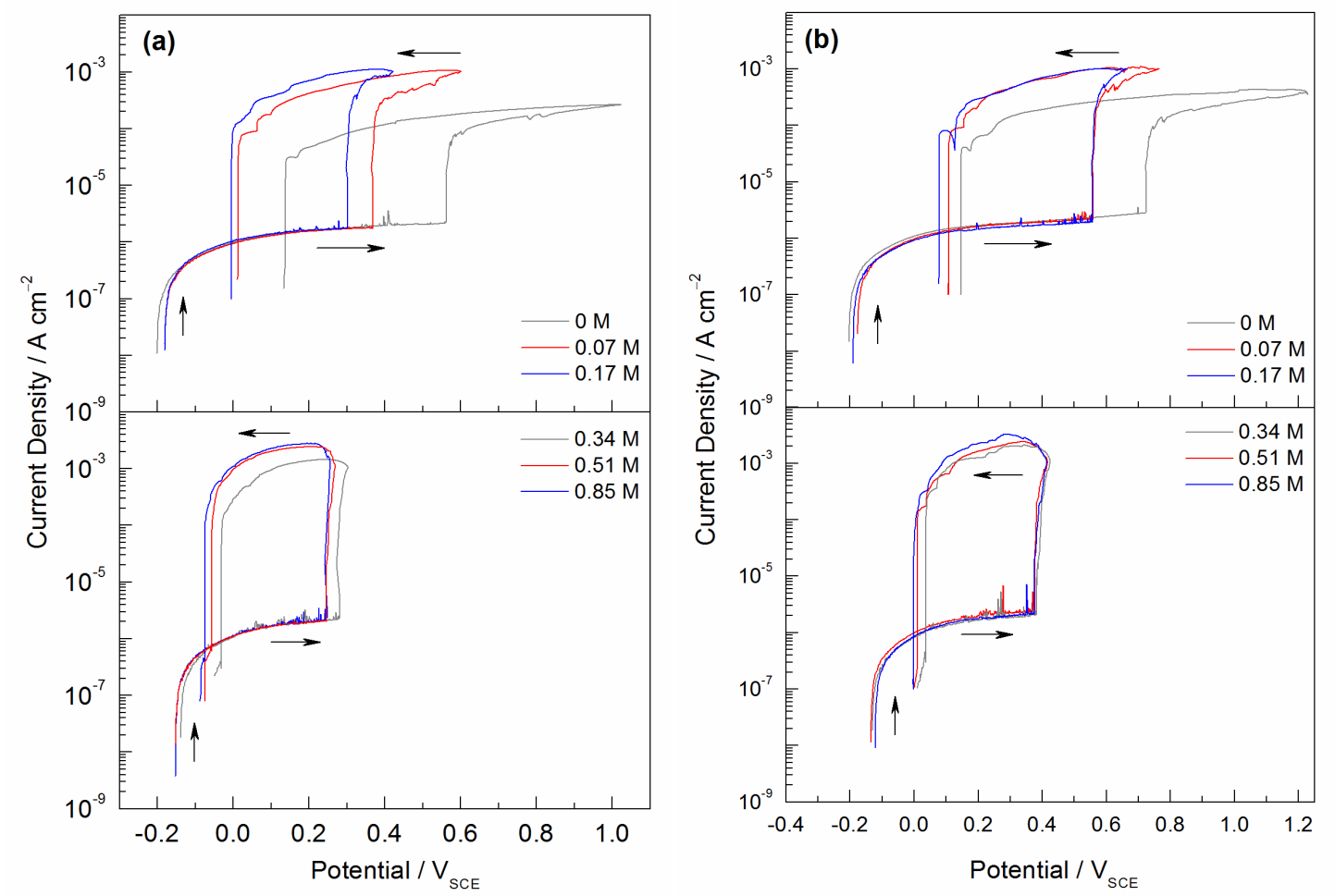

Fig. 1. Cyclic polarization curves in carbonated solution (pH=8, 25 ºC) subjected to different chloride concentrations (0, 0.07, 0.17, 0.34, 0.51 and 0.85 M) for (a) the low-nickel SS and (b) the AISI 304 SS.

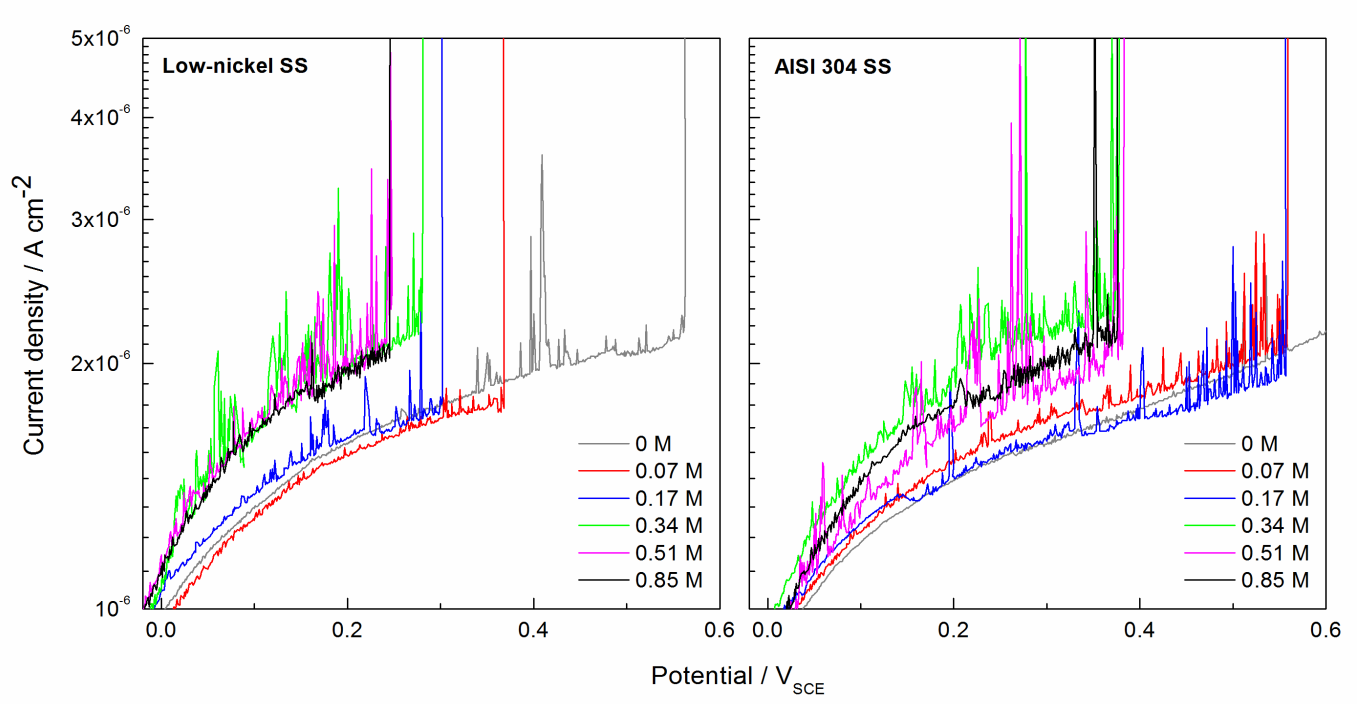

Fig. 2. Variation of the current density with the applied potential for the low-nickel SS and the AISI 304 SS in carbonated solution subjected to different chloride concentrations in the passive region.

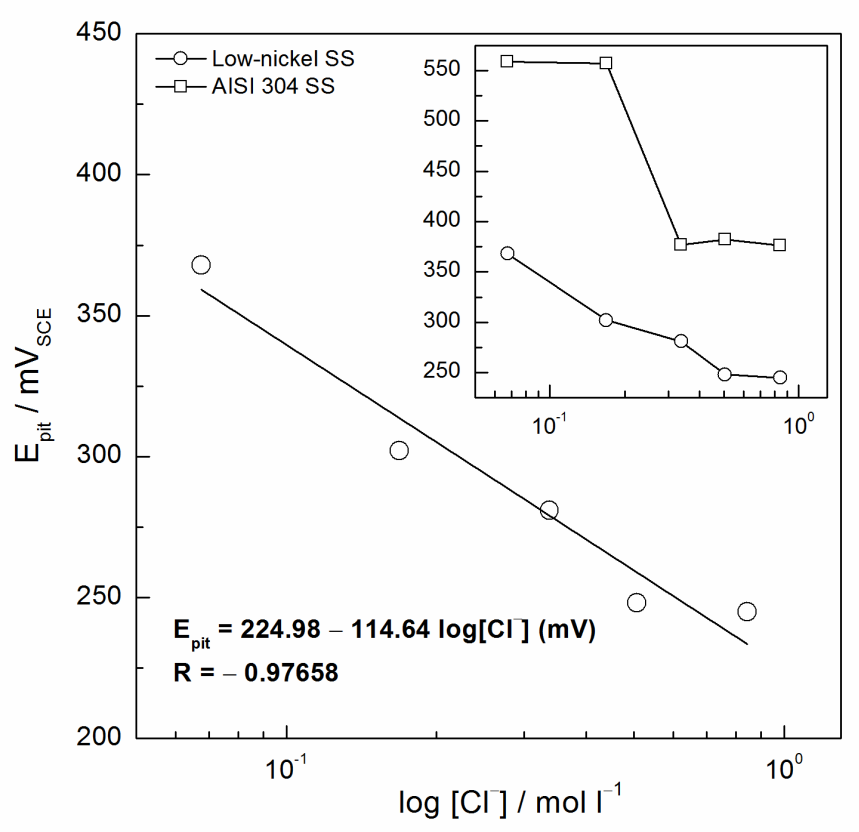

Fig. 3. Pitting potential (E_{pit}) as a function of the chloride concentration for the low-nickel SS and the AISI 304 SS in carbonated solution (pH=8, 25 ºC).

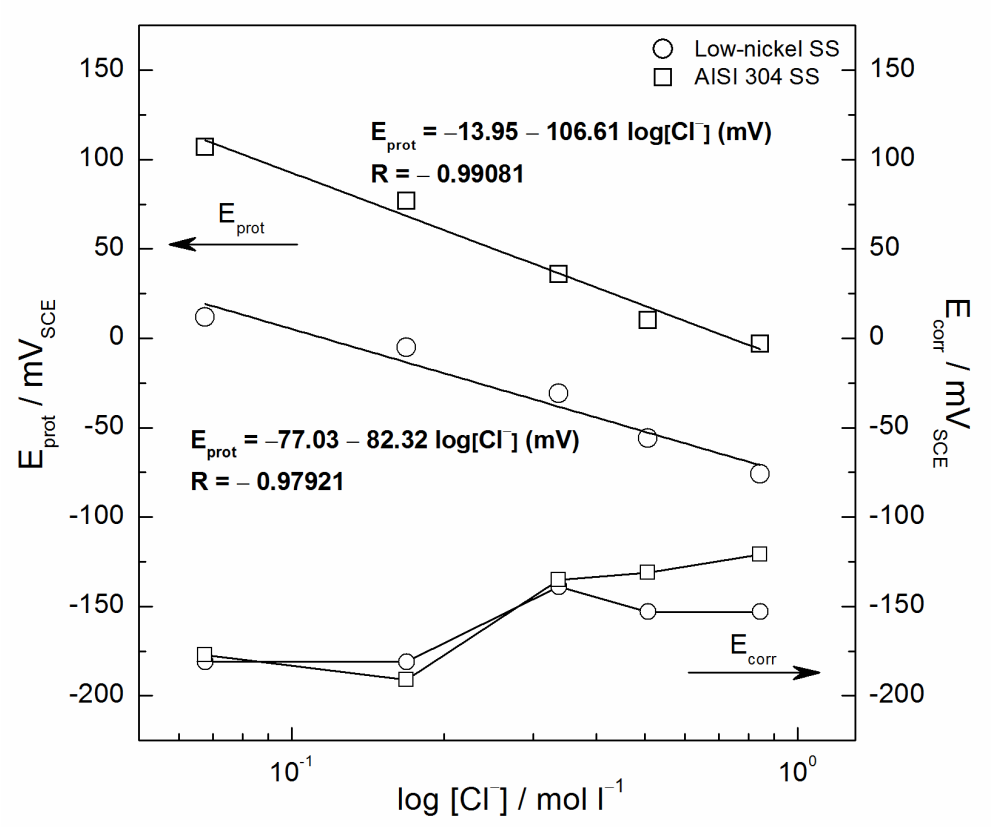

Fig. 4. Protection potential (E_{prot}) and corrosion potential (E_{corr}) as a function of the chloride concentration for the low-nickel SS and the AISI 304 SS in carbonated solution (pH=8, 25 ºC).

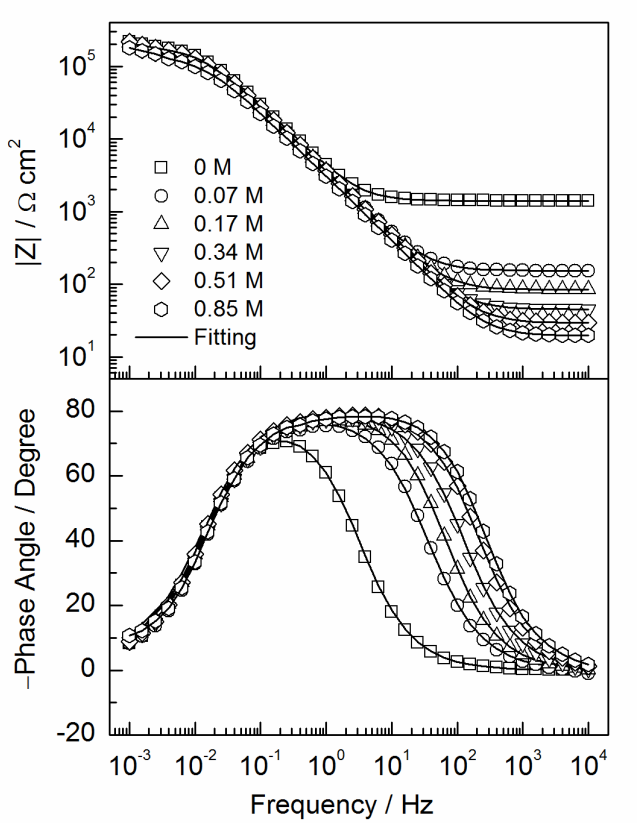

Fig. 5. Bode plots for the low-nickel SS in carbonated solution (pH=8, 25 ºC) subjected different chloride concentrations.

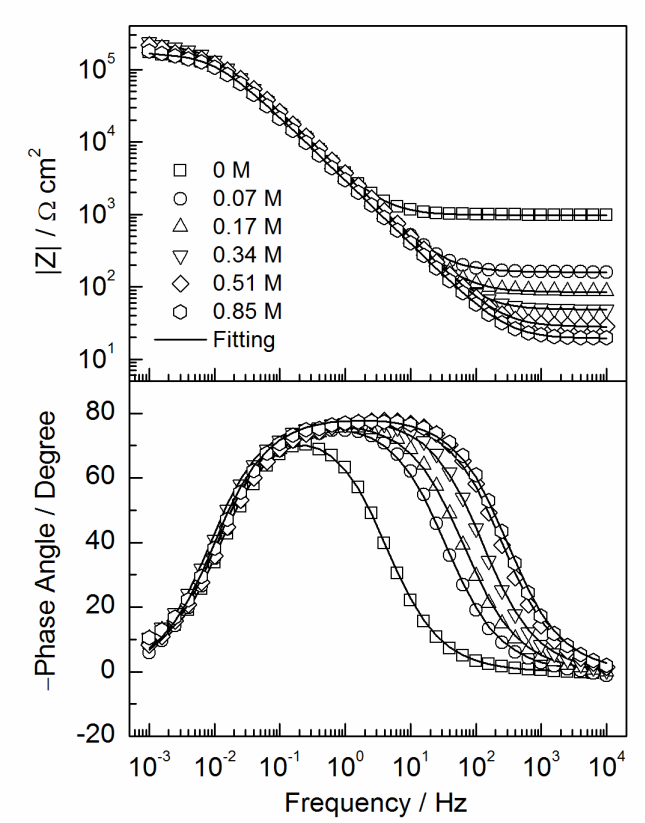

Fig. 6. Bode plots for the AISI 304 SS in carbonated solution (pH=8, 25 ºC) subjected different chloride concentrations.

.

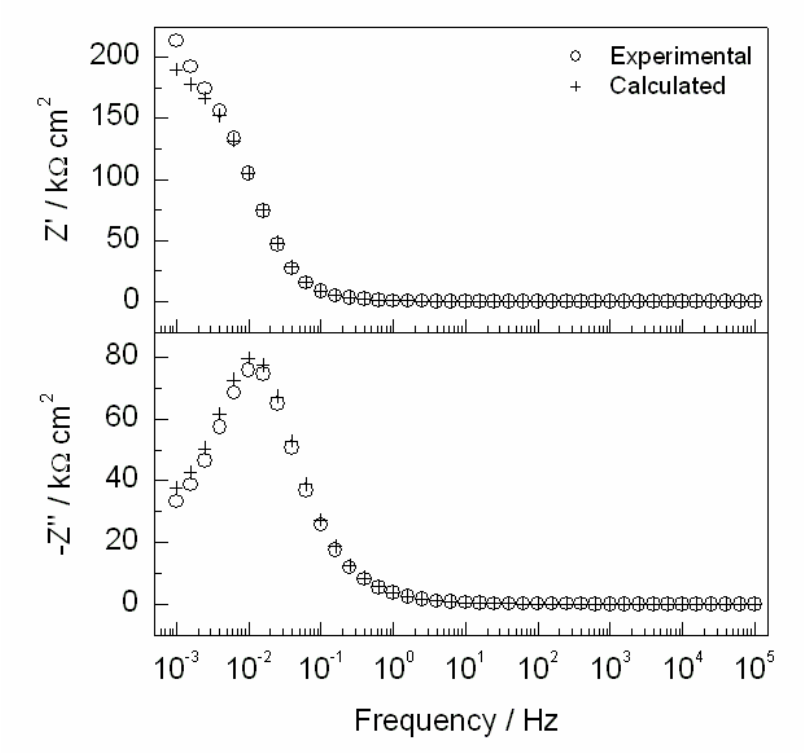

Fig. 7. Comparison of experimental impedance data (**o**) and calculated impedance data using KK transforms (**+**) for the low-nickel SS in carbonated solution (pH=8, 25 ºC), $[Cl^-]$=0.51 M.

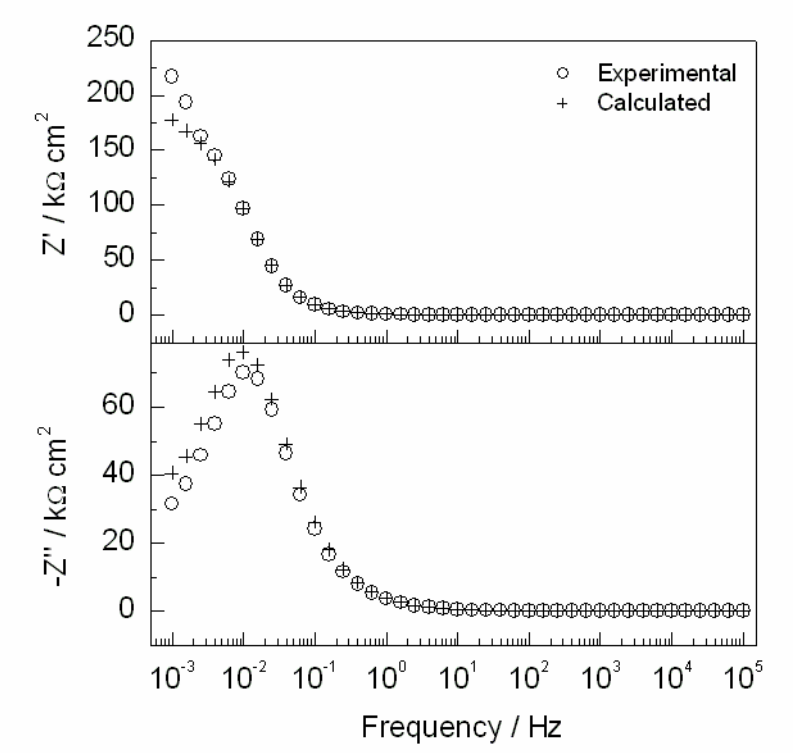

Fig. 8. Comparison of experimental impedance data (**o**) and calculated impedance data using KK transforms (**+**) for the AISI 304 SS in carbonated solution (pH=8, 25 ºC), $[Cl^-]$=0.51 M.

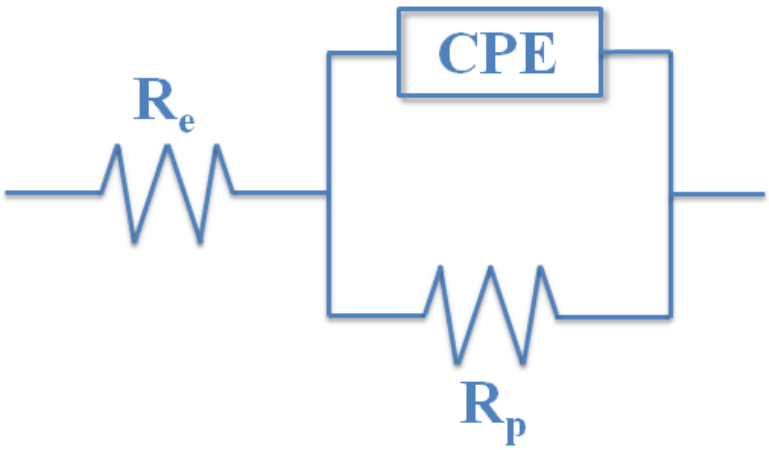

Fig. 9. Electrical equivalent circuit (EEC) used for EIS experimental data fitting for the low-nickel SS and the AISI 304 SS in carbonated solution (pH=8, 25 ºC) subjected to different chloride concentrations.

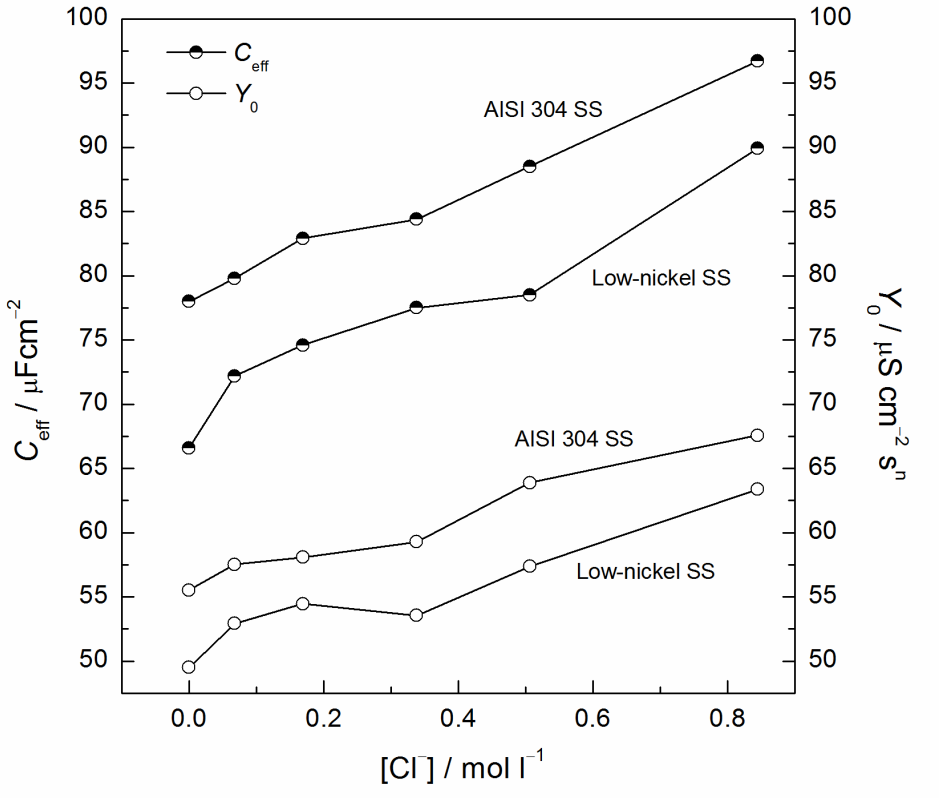

Fig. 10. Deviation of admittance (Y_0) with respect to calculated effective capacitance (C_{eff}) for the low-nickel SS and the AISI 304 SS as a function of the chloride concentration in carbonated solution (pH=8, 25 ºC).

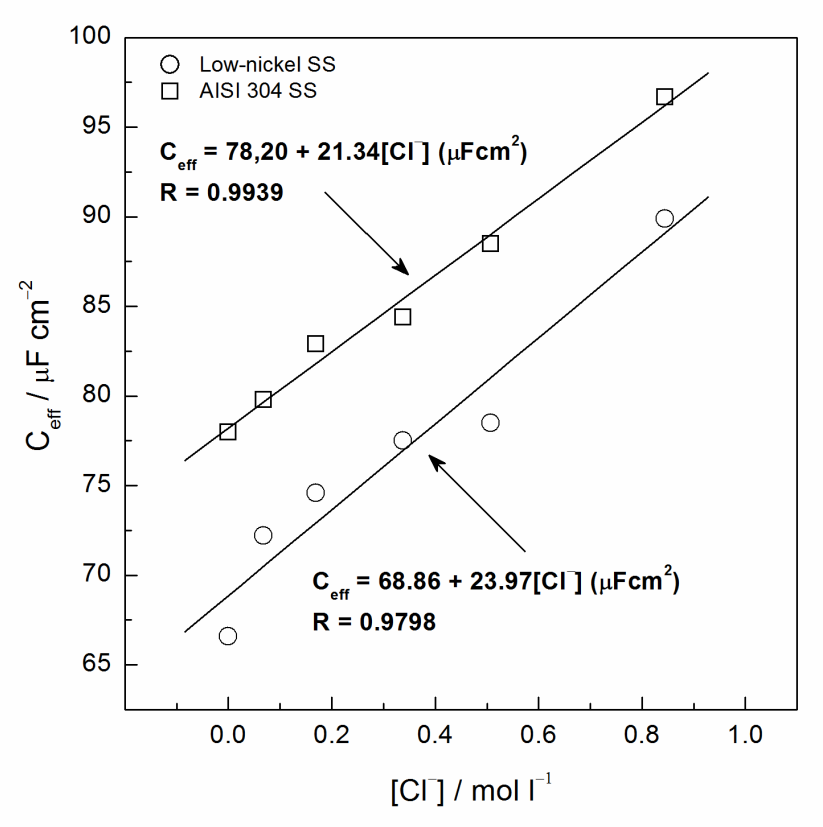

Fig. 11. Calculated effective capacitance (C_{eff}) for the low-nickel SS and the AISI 304 SS as a function of the chloride concentration in carbonated solution (pH=8, 25 ºC).

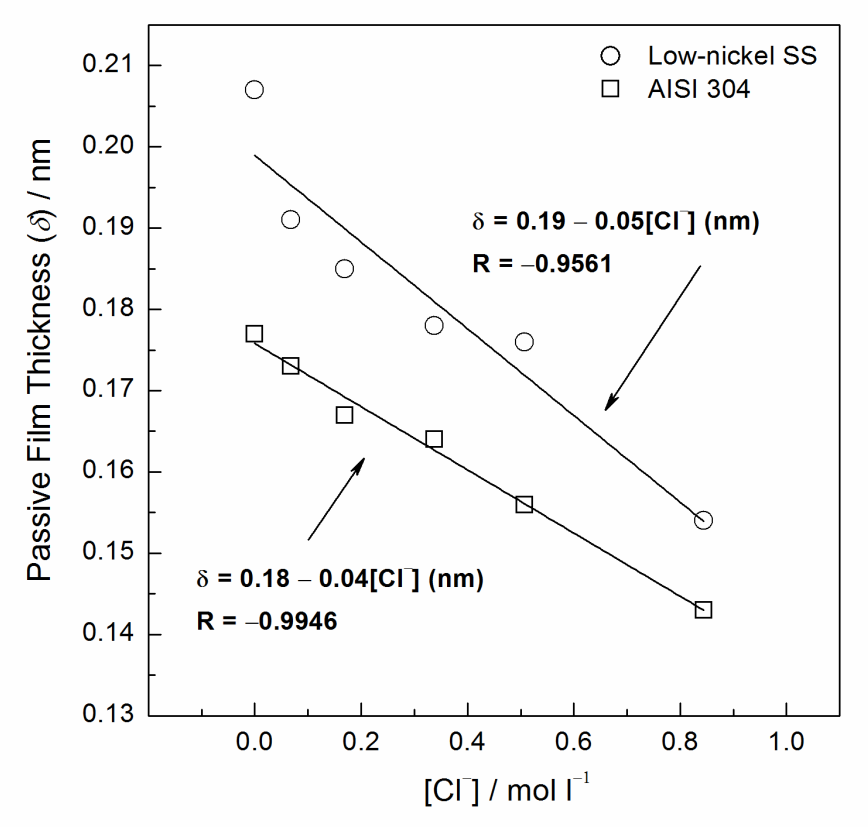

Fig. 12. Calculated passive film thickness (δ) for the low-nickel SS and the AISI 304 SS as a function of the chloride concentration in carbonated solution (pH=8, 25 ºC).

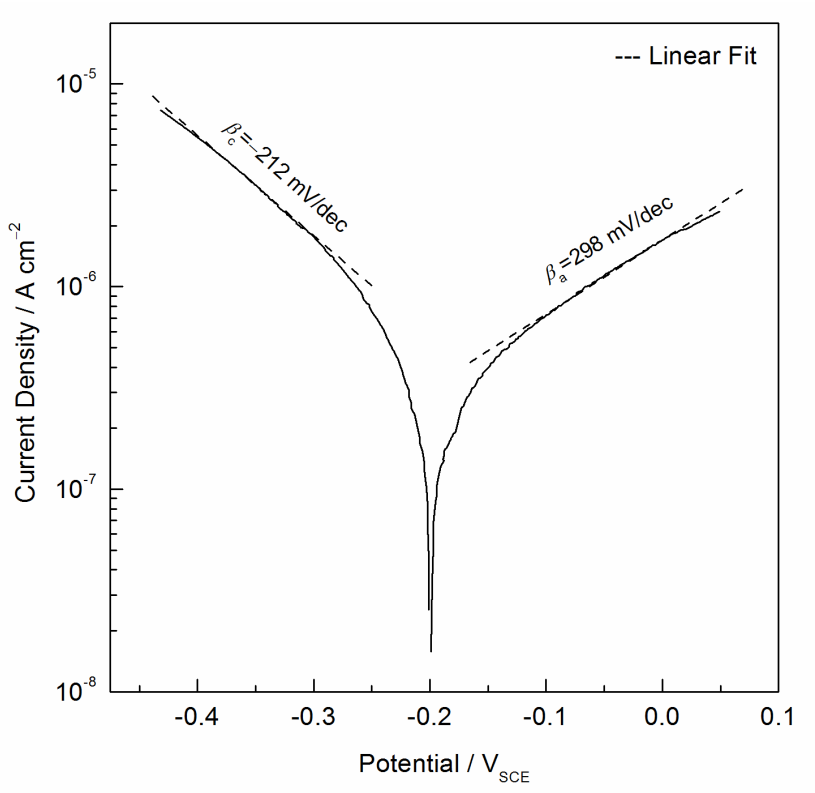

Fig. 13. Tafel slope determination for the low-nickel SS in carbonated solution (pH=8, 25 ºC), [Cl^-]=0 M.

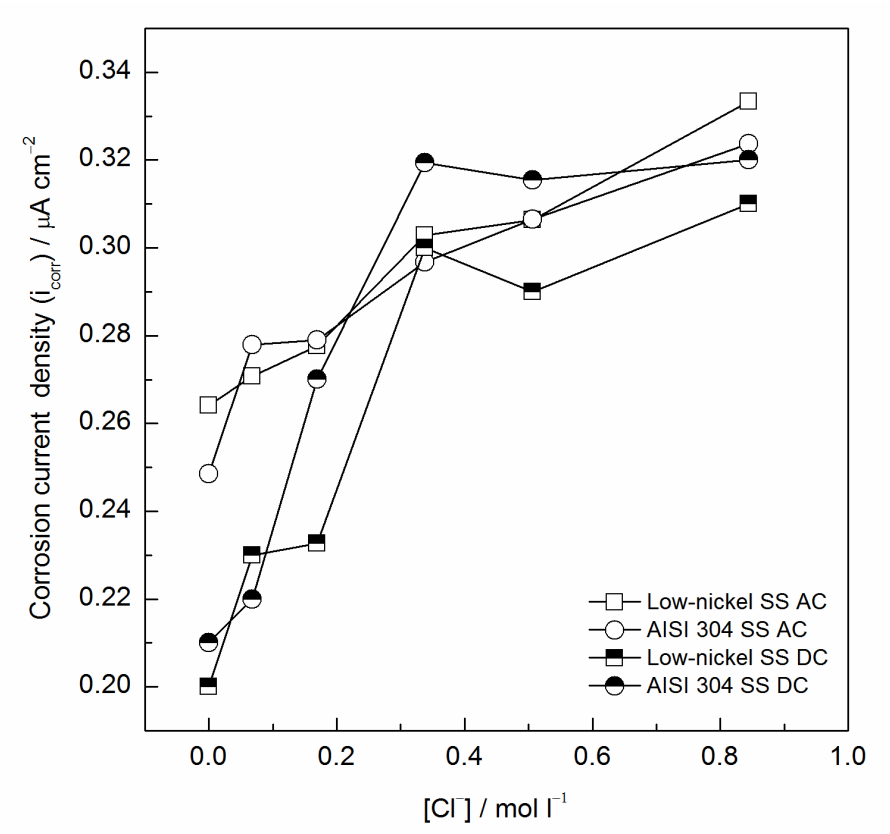

Fig. 14. Corrosion current density (i_{corr}) for the low-nickel SS and the AISI 304 SS, obtained by means of DC and AC methods, as a function of the chloride concentration in carbonated solution (pH=8, 25 ºC).